Vol. 601: 77–95, 2018
https://doi.org/10.3354/meps12685

MARINE ECOLOGY PROGRESS SERIES
Mar Ecol Prog Ser

Published August 9

Remarkable structural resistance of a nanoflagellate-dominated plankton community to iron fertilization during the Southern Ocean experiment LOHAFEX

Isabelle Schulz[1,2,3], Marina Montresor[4], Christine Klaas[1], Philipp Assmy[1,2,5], Sina Wolzenburg[1], Mangesh Gauns[6], Amit Sarkar[6,7], Stefan Thiele[8,9], Dieter Wolf-Gladrow[1], Wajih Naqvi[6], Victor Smetacek[1,6,*]

[1]Alfred-Wegener-Institut Helmholtz-Zentrum für Polar- und Meeresforschung, 27570 Bremerhaven, Germany
[2]MARUM – Center for Marine Environmental Sciences, University of Bremen, 28359 Bremen, Germany
[3]Biological and Environmental Science and Engineering Division, Red Sea Research Center, King Abdullah University of Science and Technology, 23955-6900 Thuwal, Kingdom of Saudi Arabia
[4]Stazione Zoologica Anton Dohrn, 80121 Naples, Italy
[5]Norwegian Polar Institute, Fram Centre, 9296 Tromsø, Norway
[6]CSIR National Institute of Oceanography, 403 004 Goa, India
[7]National Centre for Antarctic and Ocean Research, 403 804 Goa, India
[8]Max Planck Institute for Marine Microbiology, 28359 Bremen, Germany
[9]Institute for Inorganic and Analytical Chemistry, Friedrich Schiller University, 07743 Jena, Germany

ABSTRACT: The genesis of phytoplankton blooms and the fate of their biomass in iron-limited, high-nutrient–low-chlorophyll regions can be studied under natural conditions with ocean iron fertilization (OIF) experiments. The Indo-German OIF experiment LOHAFEX was carried out over 40 d in late summer 2009 within the cold core of a mesoscale eddy in the productive southwest Atlantic sector of the Southern Ocean. Silicate concentrations were very low, and phytoplankton biomass was dominated by autotrophic nanoflagellates (ANF) in the size range 3–10 µm. As in all previous OIF experiments, the phytoplankton responded to iron fertilization by increasing the maximum quantum yield (F_v/F_m) and cellular chlorophyll levels. Within 3 wk, chlorophyll levels tripled and ANF biomass doubled. With the exception of some diatoms and dinoflagellates, the biomass levels of all other groups of the phyto- and protozooplankton (heterotrophic nanoflagellates, dinoflagellates and ciliates) remained remarkably stable throughout the experiment both inside and outside the fertilized patch. We attribute the unusually high biomass attained and maintained by ANF to the absence of their grazers, the salps, and to constraints on protozooplankton grazers by heavy predation exerted by the large copepod stock. The resistance to change of the ecosystem structure over 38 d after fertilization, indicated by homogeneity at regional and temporal scales, suggests that it was locked into a stable, mature state that had evolved in the course of the seasonal cycle. The LOHAFEX bloom provides a case study of a resistant/robust dynamic equilibrium between auto- and heterotrophic ecosystem components resulting in low vertical flux both inside and outside the patch despite high biomass levels.

KEY WORDS: Antarctic · Protists · Fe-limitation · Si-limitation · Ecology–biogeochemistry relationship · Carbon:chlorophyll ratios · Ecosystem stability

INTRODUCTION

Pelagic ecosystem biomass inventories, i.e. the total sum of the water column standing stocks of all organisms from bacteria to top predators in units of carbon, provide the basis for assessing the trophic state of an ecosystem and its carbon sequestration potential. Information on the relative contributions of the major trophic compartments, namely phyto-, bacterio-, protozoo- and metazooplankton (Sieburth et

*Corresponding author: victor.smetacek@awi.de

Publisher: Inter-Research · www.int-res.com

al. 1978) and their various functional groups, to the total biomass in relation to nutrient availability is a prerequisite for unravelling trophic relationships and quantifying biogeochemical processes. Biomass allocation within pelagic ecosystems shifts along the trajectory of succession in the course of plankton seasonal cycles (Smetacek et al. 1984, Wassmann 1997). During the initial, new-production-based bloom phase, the rate of primary production is not limited by dissolved nutrients, and phytoplankton biomass dominates the carbon pool. Following new nutrient depletion and loss via sinking particles, regenerated nutrients mainly drive carbon fixation, and the balance between autotrophs and heterotrophs shifts accordingly: the contribution of heterotrophic biomass to total plankton biomass can be expected to increase relatively as the regenerating system establishes itself. Balance between the rate of remineralization and release of the limiting nutrient by heterotrophs (secondary producers) should now determine the rate of primary production. In its mature, nutrient-limited state, a pelagic ecosystem is ruled by the secondary producers: phytoplankton growth rates are balanced by mortality due to pathogens, parasitoids and predators (the '3 Ps') and regeneration of nutrients by them (Smetacek 2012).

Over most of the oceans and most of the year, pelagic ecosystems are characterized by the regenerating system where phytoplankton growth rates and total plankton biomass are limited by the availability of nutrients, generally nitrogen or phosphorus, but in the land-remote, high-nutrient–low-chlorophyll regions of the world ocean, the limiting nutrient is iron (Boyd et al. 2007, Moore et al. 2013). By definition, iron-limited ecosystems are characterized by regenerating plankton communities in which the rate of recycling is governed by organism interactions within complex food webs involving bacteria, various kinds of protists and metazooplankton (Landry et al. 2000a,b). Phytoplankton biomass can be below that of the combined heterotrophs (Klaas 1997). Nevertheless, chlorophyll is used as the common currency for evaluating productivity and hence also plankton standing stock in global assessments of the carbon cycle. In contrast to the vast database accumulating on global surface chlorophyll concentrations, much less information is available on the concomitant standing stocks (C m^{-2}) of other relevant components of pelagic ecosystems. This crucial information is seldom gathered because of the widespread assumption that auto- and heterotrophic biomass are correlated. However, recent models have shown that including complexities of food web interactions, such as selective grazing or predation, into biogeochemical or biodiversity models steers results along directions closer to the real world (Prowe et al. 2012, Le Quéré et al. 2016). Obviously, there is a need for more *in situ* data on the range of variability in food web biomass structure in relation to the changing environment.

The water column standing stock of particulate organic carbon (POC), which comprises both living biomass and organic detritus, is easily assessed by calibrating standard transmissometer beam attenuation profiles with discrete POC measurements made on filtered samples (Bishop 1999, Smetacek et al. 2012). The length and frequency of peaks in the profiles provide information on the size structure of the particulate pool. However, microscopy of discrete samples continues to be the most reliable technique for quantitatively assessing the ecologically relevant components of the pelagic ecosystem under study. Here we refer to 'microscopy' as the range of methods developed for visual assessment of plankton according to specific size classes of recognizable taxa or shapes, from prokaryotes to metazooplankton. Utermöhl's (1958) inverted microscope method for scanning settled water samples spans the widest size range and provides the most detailed and robust information on the state of the ecosystem. The microscopist looks directly at the foundation of the pelagic ecosystem and can count all particles of all size classes <200 µm with accuracy excepting the fraction <2 µm. The latter are accurately counted on filters under fluorescence. Indeed, the overall impression of the quantitative relationships between the ecosystem components, down to the level of recognizable taxa grouped within size classes, provided by microscopy can be compared to on-foot visual inspection of the ecosystem under study by terrestrial ecologists. Unfortunately, not many investigations have assessed the entire standing stock of protistan plankton partitioned into size classes of phylogenetic and functional groups over relevant periods of time in order to ascertain the dynamics of organism interactions and their effects on the structure and total biomass of the respective pelagic ecosystem.

Ocean iron fertilization (OIF) experiments provide the necessary conditions to follow the quantitative and qualitative effects of alleviation of a limiting resource on all components of the ecosystem and compare them with unaffected surrounding waters. Here we present results on the impact of OIF on the composition and biomass of the protistan community during the 40 d Indo-German experiment LOHAFEX ('loha': Hindi term for iron, FEX: fertilization experiment). The experiment was carried out during late

summer in the productive south-west (SW) Atlantic sector of the Antarctic Circumpolar Current (ACC). This region receives more iron from various sources than the rest of the ACC where the previous Southern Ocean OIF experiments SOIREE, EisenEx, SOFEX North and South patches and EIFEX were conducted (Boyd et al. 2007). The sources of iron are from Patagonian dust, from sediments and runoff from the Antarctic Peninsula and its associated islands (including South Georgia; Borrione et al. 2014), from fossil dust released from melting icebergs (Raiswell et al. 2008, Wadley et al. 2014), upwelling and even from hydrothermal vents (Resing et al. 2015). As a result of the higher productivity, silicate concentrations in the surface layer of the Antarctic Zone south of the Polar Front are depleted to very low levels by mid-summer (Sarmiento et al. 2004). However, elevated chlorophyll concentrations are still present in the late summer season (Venables & Meredith 2009, Hoppe et al. 2017), but the composition of the plankton and its response to natural iron fertilization are poorly known.

Productivity of the Southern Ocean has played a key role in modulating atmospheric CO_2 levels over past glacial cycles (Martin 1990) and diatoms are believed to be the main vehicles of deep vertical flux (Abelmann et al. 2006, Tréguer et al. 2018). However, the entire ACC north of the Polar Front becomes silicate limited by late summer, so ascertaining the effect of iron input to these waters is of relevance for understanding the global carbon cycle of past, present and future oceans. The overall aim of LOHAFEX was to study the effect of iron fertilization on the biological carbon pump of silicate-limited water over a prolonged period. In order to ensure sufficient longevity of the fertilized patch, the experiment was carried out in the closed core of a mesoscale eddy formed by the meandering Antarctic Polar Front (Martin et al. 2013). The same technique was successfully employed in the 2 previous experiments EisenEx (21 d) and EIFEX (37 d) that were able to track the intact patch for the entire duration of the experiments (Gervais et al. 2002, Assmy et al. 2007, Smetacek et al. 2012). The movement and behaviour of the patch during LOHAFEX as well as the export flux have been presented by Martin et al. (2013) and Ebersbach et al. (2014). The bacterioplankton composition, abundance and biomass were reported by Thiele et al. (2012, 2014). The composition, biomass and feeding behaviour of metazooplankton were also investigated (H. E. Gonzalés unpubl. data, M. G. Mazzocchi et al. unpubl. data). Here we present and discuss the dynamics of the protist community inside and outside the patch based on microscopy of live plankton on board and subsequent detailed cell counts of preserved samples.

MATERIALS AND METHODS

LOHAFEX experiment

The LOHAFEX experiment was carried out from 26 January to 6 March 2009 (40 d) in the SW Atlantic sector of the Southern Ocean during RV 'Polarstern' cruise ANT-XXV/3. The experimental mesoscale cyclonic eddy was located at approximately 48° S, 16° W, enclosed by a meander of the Antarctic Polar Front. The centre of the eddy core was marked with a GPS-equipped, surface-tethered buoy and the initial station (Day −1) sampled adjacent to it on 26 January 2009. A circular patch of 20 km diameter (300 km^2) around the buoy was fertilized with 10 t of dissolved iron (II) sulphate heptahydrate (10 t $FeSO_4 \cdot 7 H_2O$ corresponding to 2 t of iron) to yield a theoretical concentration of 2 nM Fe on 27 January (Day 0). On Day 20, the patch was again fertilized with 10 t of $FeSO_4$. 'Inside stations' were located in the centre of the patch, the location of which was determined using online measurements of maximum quantum yield (F_v/F_m), underway chl *a* sampling and continuous pCO_2 measurements. 'Outside stations' were located within the closed core but as far as possible from the border of the spreading patch until the eddy collapsed. A few stations with properties in between inside and outside stations (termed 'edge stations') were not included in the statistical analyses. For details of patch dynamics, see Martin et al. (2013).

Sampling and analytical procedures

The mixed layer (80 m, Martin et al. 2013) was sampled at each station with multiple casts of a conductivity, temperature, depth rosette (SeaBird Electronics) equipped with a profiling Wet Labs C-Star transmissometer (660 nm wavelength) and 12 l Niskin bottles. For measurement of POC, 2 l were filtered on pre-combusted Whatman GF/F filters and analysed with a EURO3000 Eurovector elemental analyser. Integrated stocks of POC were derived from transmissometer profiles calibrated against discrete measurements as described by Smetacek et al. (2012). For chl *a* measurements, 1 l of seawater was filtered onto GF/F filters. Filters were immediately transferred to centrifuge tubes with 10 ml 90% ace-

tone and 1 ml of glass beads, sealed and stored at −20°C for at least 30 min and up to 24 h. Chl *a* was extracted by grinding the filters in a cell mill followed by centrifugation and analysis of the supernatant with a Turner 10-AU fluorometer following the JGOFS protocol procedure (Knap et al. 1996). Phyto- and microzooplankton samples were taken from 5 discrete depths (10, 20, 40, 60, 80 m) prior to iron fertilization (Day −1), at 11 stations inside the patch, 4 stations outside the patch and 1 station in between (edge patch).

Microscopic investigation of the protist community

Cells were identified and enumerated under an inverted light microscope equipped with epifluorescence (Axiovert 200 and Axio Observer 1.0) according to Throndsen (1995). To determine pico- and nanoplankton abundance and biomass, Lugol-preserved water samples were settled in 10 ml sedimentation chambers (Hydrobios) for 24 h. Flagellate and coccoid cells lacking distinctive morphological features were counted in 3 size categories: <3, 3–6 and 6–20 µm. The haptophyte *Phaeocystis antarctica* was counted in 2 size categories: 2–4 and 4–6 µm. More distinct flagellates generally >6 µm could be identified to species level (e.g. *Leucocryptos marina*) using scanning electron microscopy (SEM). SEM preparations were made at the Stazione Zoologica in Naples, Italy, following the methods described by Zingone et al. (2011), and observed using a JEOL JSM-6700 SE Filter SEM (JEOL-USA).

To determine microplankton (protists >20 µm) and coccolithophores, hexamethylenetetramine-buffered formaldehyde-fixed water samples (2% final concentration) were settled in 50 ml sedimentation chambers for 48 h. Depending on their size and abundance, organisms were counted at 50–200× magnification in transects to cover a quarter, half or complete Utermöhl chamber. In order to obtain a statistically robust result from the quantitative analyses, samples were analysed until at least 50 cells of the most abundant species and in total 500 cells were counted.

To estimate the composition and biomass of large protozooplankton and copepods <1 mm, the whole content of 1 Niskin bottle (12 l) was gently sieved onto 20 µm mesh gauze and concentrated to a final volume of 50 ml. Samples were fixed with hexamethylenetetramine-buffered formaldehyde (2% final concentration) and 2 ml of a strontium chloride solution ($SrCl_2 \cdot 6H_2O$; Beers & Stewart 1970) to prevent dissolution of acantharian skeletons. The entire sample for each depth was settled in a 50 ml sedimentation chamber (Hydrobios) at 4°C for 48 h and examined under an inverted microscope. Naked ciliates are not retained quantitatively by the 20 µm gauze (Smetacek 1981) and were therefore counted in Lugol-fixed samples (see above). In total, 10 functional groups could be distinguished: loricate (tintinnid) ciliates, athecate (naked) and thecate (armoured) dinoflagellates, silicoflagellates, copepods <1 mm and Foraminifera, Acantharia, Heliozoa and Radiolaria (the latter 4 taxa categorized under Rhizaria).

To estimate plankton biomass, cell size of each species or category was measured on 20 randomly chosen cells, and their biovolume was calculated from equivalent geometrical formulas (Hillebrand et al. 1999). The biovolumes were then converted into cellular carbon contents using carbon conversion factors for specific plankton groups after Menden-Deuer & Lessard (2000). Carbon conversion factors for nauplii and small copepods, counted in size classes, were taken from Henjes et al. (2007a) and bacterial biomass was taken from Thiele et al. (2012).

Regression analysis and hypothesis tests were carried out using the statistics toolbox in MATLAB®. Count uncertainties, estimated assuming a random distribution of cells in the counting chambers (Zar 1999), are always given as 1 SD.

RESULTS

Environmental setting

The LOHAFEX eddy was located at the tail end of the continuous plume of enhanced chlorophyll concentration downstream from South Georgia (Fig. 1a). During the first 3 wk, the eddy remained stable and the fertilized patch completed 2 rotations while spreading in size within the eddy core; the effects of dilution in the centre of the patch, where inside stations were sampled, will have been minor in this period. At the beginning of the fourth week, the eddy collapsed, which resulted in elongation and dilution of the patch during its southward displacement to a new stable position where it remained during the last 10 d (Martin et al. 2013). Frequent storms with maximal wind speeds of 11 m s^{-1} resulted in intermittent mixing of the surface layer that deepened from initially 60 to 80 m by the end of the experiment (Smetacek & Naqvi 2010). Combined nitrite and nitrate concentrations decreased linearly from an

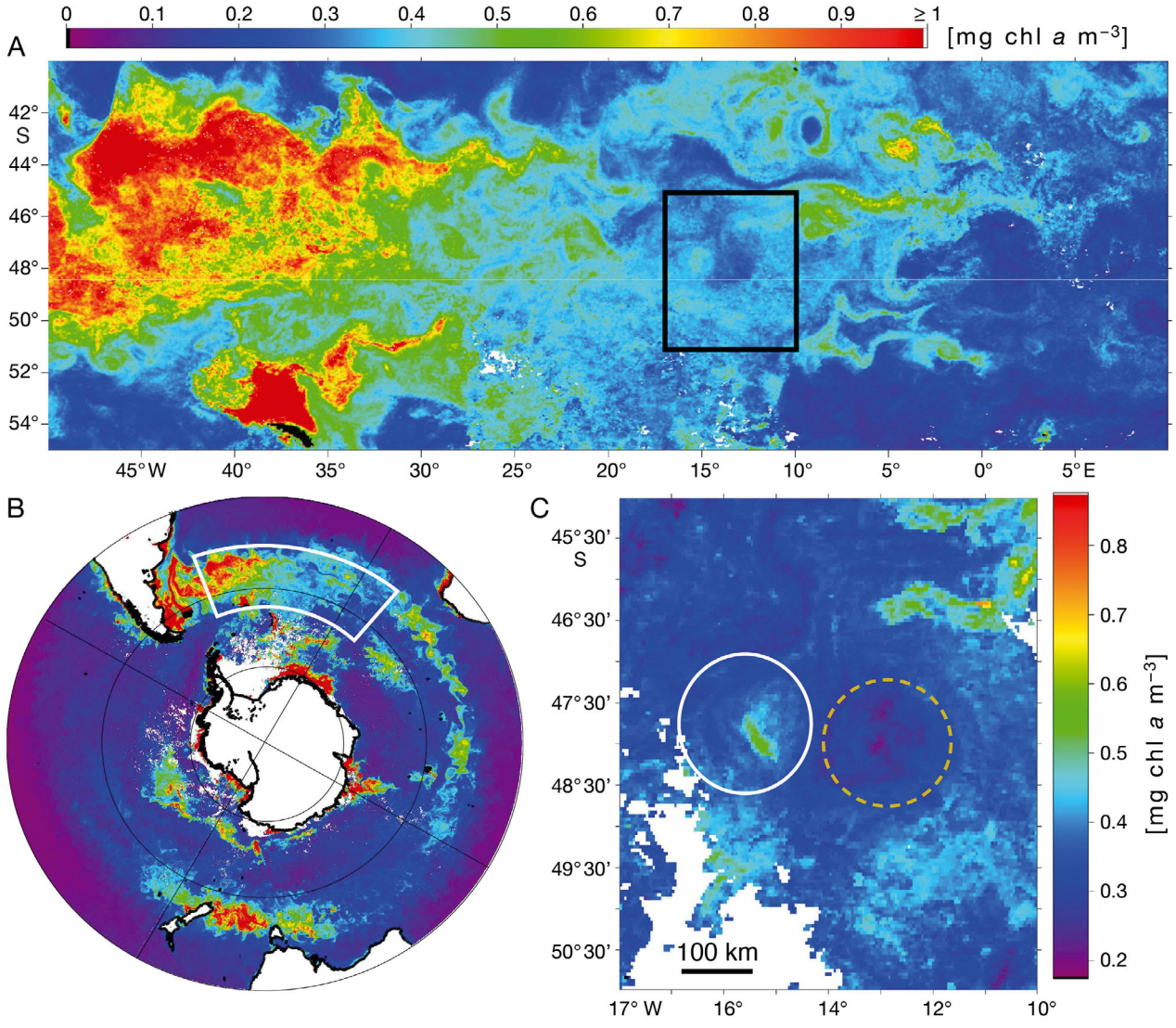

Fig. 1. Satellite-derived surface chl *a* concentrations of the region of enhanced productivity stimulated by iron input from South Georgia (bottom of panel A) from the Ocean Colour Climate Change Initiative (Sathyendranath et al. 2018). (A) February monthly climatology (the black box outlines the location of the LOHAFEX eddy, magnified in panel C). (B) Overview of chl distribution of the entire Southern Ocean in February 2009. The white box is the region magnified in panel A. Colour scales are the same for A and B (C) Surface values between 10 and 15 February 2009. The LOHAFEX eddy (encircled with a white ring) and the growing bloom in its core on Day 14 of the experiment are clearly visible. Also prominent is the impoverished core of the adjacent counter-clockwise rotating eddy (encircled with a dashed line) that can be traced to the band of low-chlorophyll water north of the Polar Front

upper mixed layer average of ~20 µM at the beginning of the experiment to 16 µM inside the patch and 17 µM outside of it. Ammonium concentrations averaged 0.9 ± 0.4 µM inside and 0.9 ± 0.3 µM outside, with no sign of a trend. Silicate concentrations, ranging from 0.5 to 2 µM, were at the limit of detection of the method throughout and showed no significant trend inside or outside the patch.

Prior to fertilization, maximum quantum yield (F_v/F_m) measured continuously in water from 10 m depth with a fast repetition-rate fluorometer was low (~0.33) and increased within the first 6 d, reaching its maximum (>0.5) on Day 14, and remained distinctly above outside values until the end of the experiment (Martin et al. 2013). Chl *a* standing stocks for the 80 m water column increased almost 3-fold from 34–40 mg m^{-2} at the beginning of the experiment to 90 mg m^{-2} on Day 22 (Fig. 2). The highest chl *a* concentration measured during LOHAFEX was 1.7 mg chl *a* m^{-3}. Stocks declined thereafter to average val-

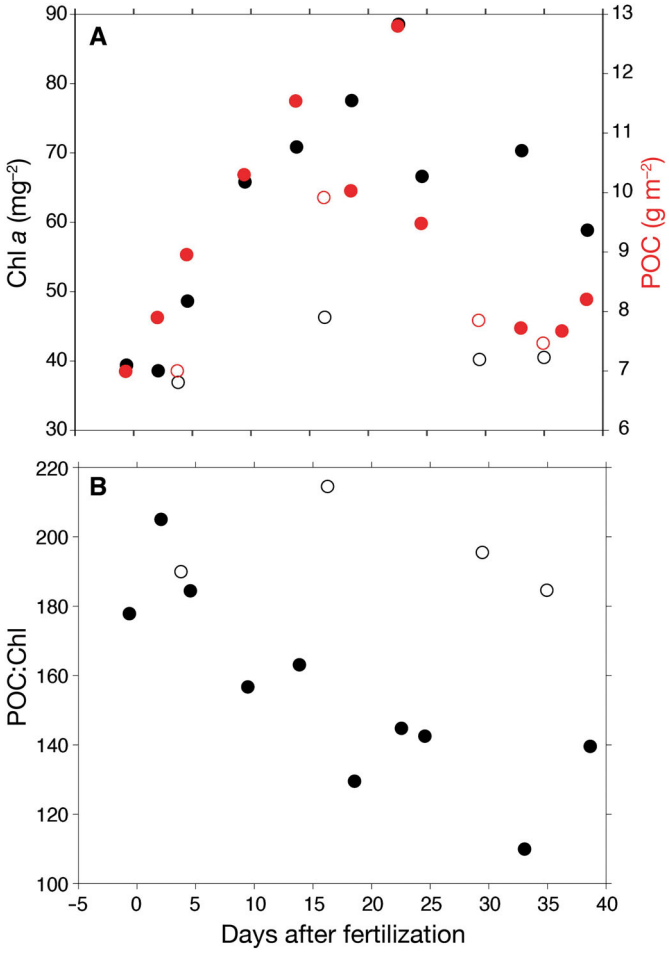

Fig. 2. (A) Time courses of the 80 m integrated stocks of particulate organic carbon (POC, red dots) and chl *a* (black dots) and (B) POC:chl ratio inside and outside the iron-fertilized patch (see Fig. 1) over the 40 d experiment. Filled and open circles represent stations inside and outside the patch, respectively

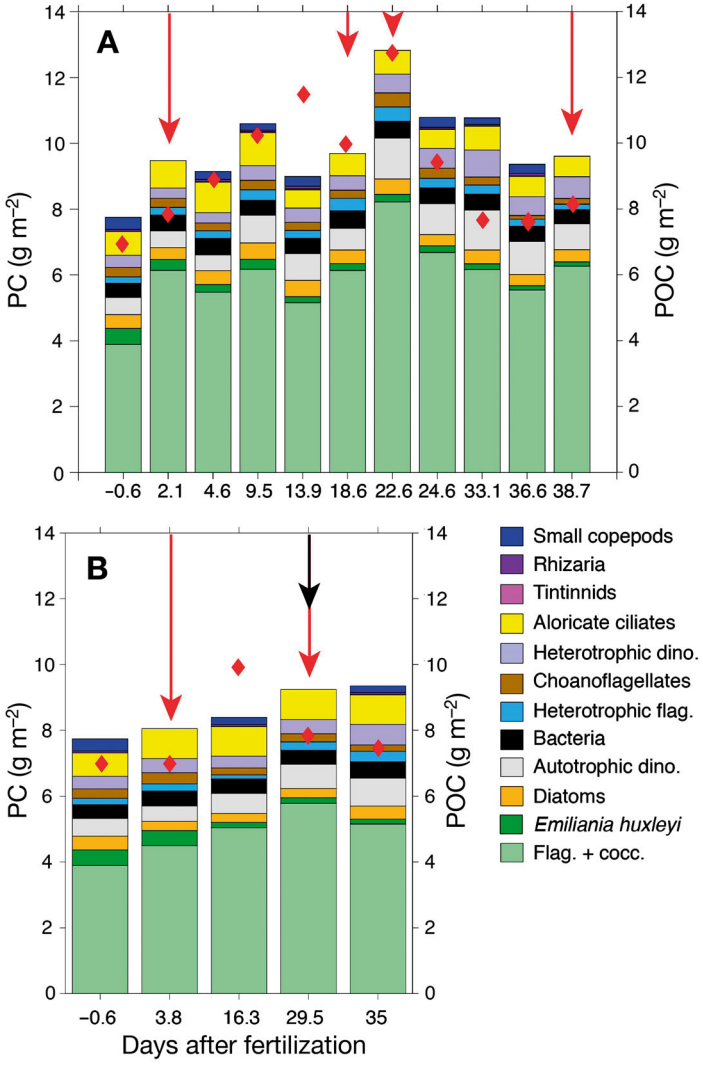

Fig. 3. Total plankton carbon (PC, bars, derived from cell counts) and particulate organic carbon (POC, red diamonds) stocks (A) inside and (B) outside the iron-fertilized patch (see Fig. 1). Flag. + cocc. = autotrophic nanoflagellates and coccoid cells. Autotrophic dino. = autotrophic dinoflagellates. Heterotrophic flag. = heterotrophic nanoflagellates. Heterotrophic dino. = heterotrophic dinoflagellates. Rhizaria comprise Foraminifera, Acantharia and Radiolaria. Small copepods (< 1mm) include nauplii and copepodites. Tintinnids, Rhizaria and small copepods were counted in 12 l concentrated samples that were not taken at the stations marked with the red arrows. The black arrow indicates the edge station

ues of 65 ± 6 mg chl *a* m^{-2} (0.82 ± 0.07 mg chl *a* m^{-3}), still significantly (*t*-test, $t = 6.66$, df = 5, $p = 0.0012$) above outside values which showed little variation, averaging 41 ± 4 mg chl *a* m^{-2} (0.51 ± 0.05 mg chl *a* m^{-3}; Fig. 2) throughout the 40 d. POC increased from initially 7 g C m^{-2} to its maximum on Day 22 at 13 g C m^{-2}. The mean POC value outside the patch was 8.4 ± 1.2 g C m^{-2}. Variation in POC and chl *a* stocks in the first 3 wk are probably due to our missing the hotspot at some stations inside the patch. The peak on Day 22 indicates that there was still relatively undiluted patch water present in the hotspot until this time.

POC and chl *a* concentrations were highly correlated both inside and outside the patch (see Fig. S1 in the Supplement at www.int-res.com/articles/suppl/m601p077_supp.pdf): POC = 110 chl *a* + 18 (r^2 = 0.898; $p < 0.001$) and POC = 157 chl *a* + 8 ($r^2 = 0.957$; $p < 0.0001$), respectively. The POC:chl *a* ratio for the discrete values was much lower inside as compared to outside the patch and decreased 2-fold within the first 2 wk after fertilization (from 200 to 100) and stabilized thereafter (Fig. 2b). Ratios in outside waters were around 175:1. Primary productivity derived from ^{14}C bottle incubations increased within the

patch to a maximum of 1.6 g C m^{-2} d^{-1} and remained below 1 g C m^{-2} d^{-1} outside the patch (M. Gauns unpubl. data).

Plankton biomass

The biomass standing stocks in g C m^{-2} derived from organism counts of the entire protist plankton community <200 µm integrated for the 80 m surface layer of 11 stations inside the patch, 4 outside and 1 edge station are depicted in Fig. 3. The histograms include the biomass of all protists counted in water samples and, at most stations, the biomass of larger, robust organisms (mostly Rhizaria and copepod larvae) counted in 12 l samples concentrated by 20 µm mesh net. Concentrated samples for the larger organisms were not taken at stations marked with a red arrow; since their biomass contribution was always below 5%, the effect on total plankton biomass is negligible. Total plankton biomass inside the patch increased from 7.8 to 12.9 g C m^{-2} on Day 23, concomitant with stocks of POC and chl *a*. Phytoplankton biomass accounted for 75 ± 3% of total biomass inside and 70 ± 2% outside the fertilized patch. The contributions of bacteria (Thiele et al. 2012) and protozooplankton to total biomass were 5.9 ± 0.6 and 18 ± 2%, respectively. Outside the patch, the contributions of heterotrophic bacteria and protozooplankton were 5.5 ± 0.2% and 22 ± 2%, respectively. Bacterial biomass remained stable, with mean values of 0.48 ± 0.03 and 0.43 ± 0.08 g C m^{-2} for inside and outside stations, respectively (Thiele et al. 2012).

Measured POC stocks were almost always somewhat lower than the plankton carbon (PC) estimated with microscopy, indicating over-estimation of the latter. Since detritus particles including faecal material were not included in the counts, the overestimation of PC will be even greater than indicated in the figure. However, regression analysis of all discrete values from all stations of POC and PC were highly correlated (r^2 = 0.709; $p < 0.001$) with a slope of 0.9, indicating that the overestimation by about 10% did not affect observed trends in total PC. As the bulk of the biomass was present in the nanoflagellate and coccoid-cell size classes 3–6 and 6–20 µm, the most likely explanation for the higher biomass levels derived from counts relative to measured POC levels is an overestimation of the volume of the counted cells due to the broad size classes in which cells were assigned. It is also evident from Fig. 4 that the temporal variation in total biomass is mainly due to the 3–20 µm size class. Since there was little temporal change in protist size categories, the error will have been systematic.

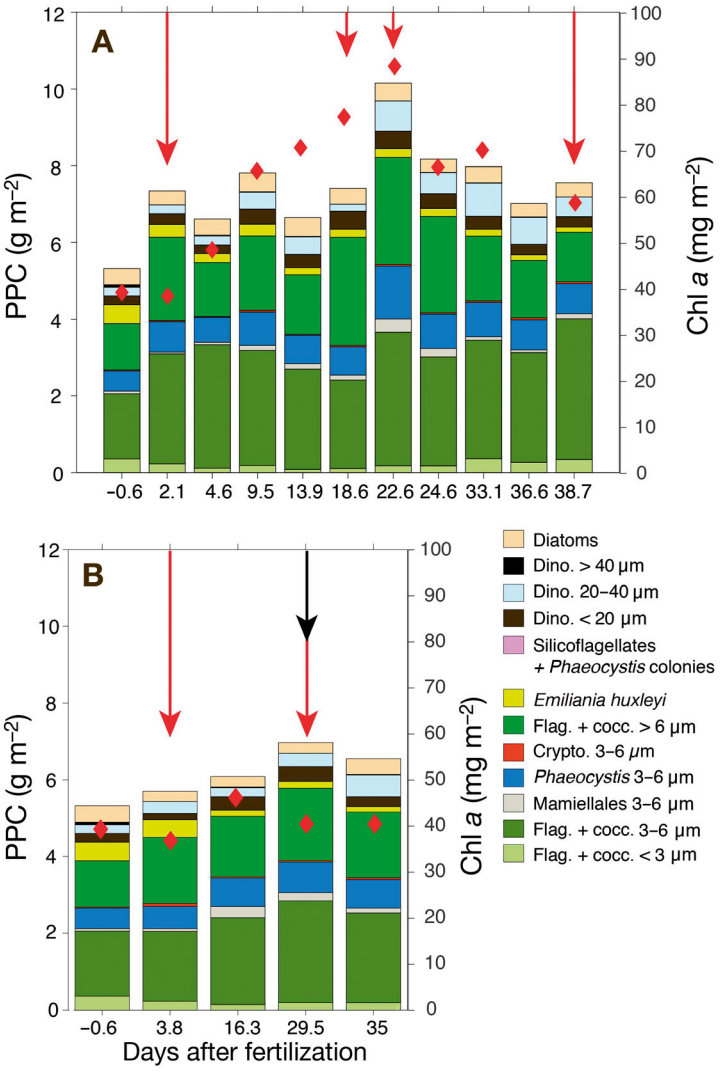

Fig. 4. Total phytoplankton carbon (PPC, bars) and chl *a* (red diamonds) stocks (A) inside and (B) outside the iron-fertilized patch (see Fig. 1) integrated for the 80 m surface mixed layer in g C m^{-2} with the contributions of autotrophic nanoflagellates (flagellate and coccoid chlorophyll-bearing cells = Flag. + cocc.) in the size classes <3, 3–6 and >6 µm, flagellates belonging to the Mamiellales (3–6 µm), solitary Phaeocystis cells (3–6 µm), cryptophytes (Crypto. 3–6 µm), autotrophic nanoflagellates >6 µm (Flag. + cocc. >6 µm), *Emiliania huxleyi*, combined silicoflagellates and *Phaeocystis* colonies, autotrophic dinoflagellates (Dino.) in size classes <20, 20–40 and >40 µm and diatoms. Red arrows indicate stations where larger protozoa (mostly Rhizaria) and copepod counts (from 12 l concentrated water samples) were not available. The black arrow indicates the edge station. See also Fig. 2 in the Supplement

Phytoplankton biomass (PPC) with the relative contributions of the various groups are presented in Fig. 4 together with chl *a* stocks. The correlation be-

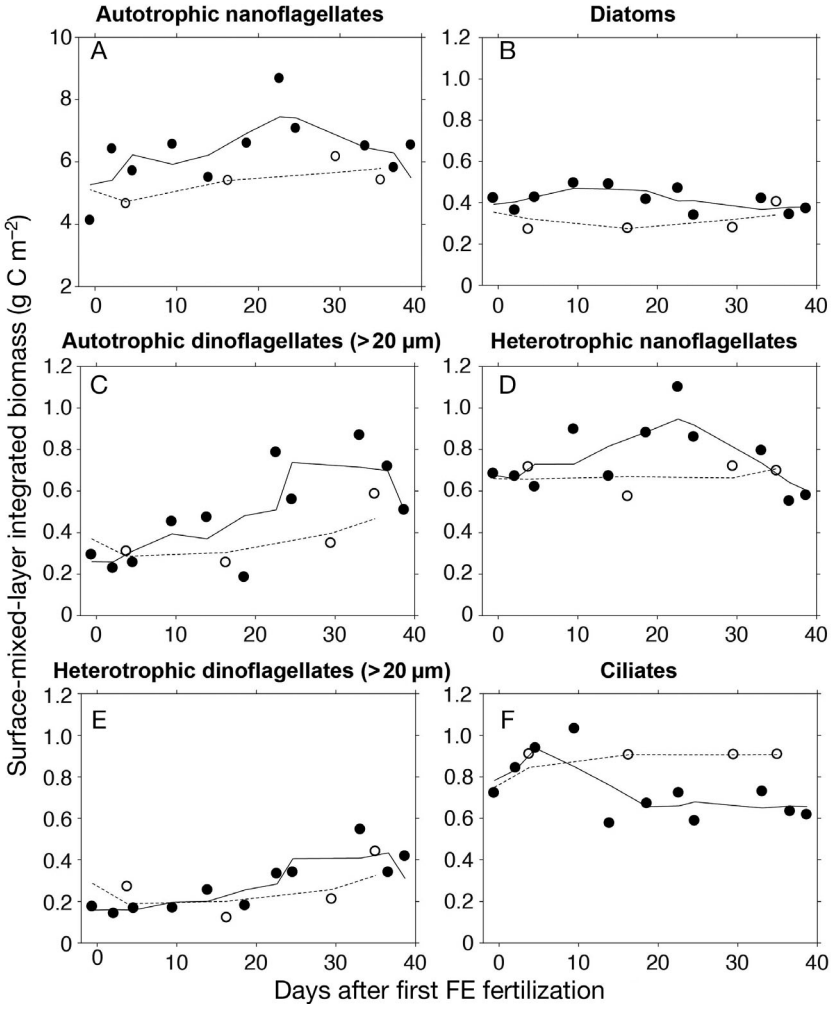

Fig. 5. Time courses of the biomass stocks integrated for the 80 m surface mixed layer in g C m^{-2} of all size classes of (A) autotrophic nanoflagellates, (B) diatoms, (C) autotrophic dinoflagellates >20 µm, (D) heterotrophic nanoflagellates, (E) heterotrophic dinoflagellates >20 µm and (F) all ciliates inside (filled circles) and outside the iron-fertilized patch (open circles) (see Fig. 1), showing differences in, or lack of, response to iron fertilization. Autotrophic and heterotrophic dinoflagellates <20 µm are included with the respective nanoflagellates

tween PPC and chl *a* for all in-patch discrete values was high (r^2 = 0.785) with a slope of 65 ± 10 (mean ± 95% CI) and intercept of 36 ± 9 mg m^{-3} (mean ± 95% CI). The PPC to chl *a* correlation for out-patch stations was even higher (r^2 = 0.945) with a slope of 145 ± 29 (mean ± 95% CI) and intercept of 0 ± 16 mg m^{-3} (mean ± 95% CI). The bulk of the PPC was contributed by autotrophic nanoflagellates, including coccoid cells, in the size classes 3–6 and 6–20 µm (80 ± 3% and 78 ± 4% inside and outside the patch, respectively). Their peak values were reached on Day 23: 5.4 and 2.8 g C m^{-2}, amounting to 42 and 22% of total plankton biomass, respectively (Fig. 5). The smallest size class (<3 µm) was the most abundant, but its biomass was only 0.18 g C m^{-2} on Day 23.

A number of nanoflagellate taxa could be identified with confidence in light microscopy counts of Lugol-fixed samples, in particular the haptophyte flagellate cf. *Phaeocystis antarctica* on the basis of its characteristic heart shape, the presence of 2 chloroplasts and often the 2 flagella and the haptonema. The solitary cells of this species accounted, on average, for 0.83 ± 0.23 mg C m^{-2} inside the fertilized patch and 0.70 ± 0.11 mg C m^{-2} outside the patch (Figs. 4 & 6). *Phaeocystis* colonies were recorded only during the first part of the bloom, up to Day 23, and represented a negligible fraction of the phytoplankton carbon. Early stages of colony formation attached to spines of the diatom *Corethron pennatum*, chains of *Pseudonitzschia* or other diatom species were common only in the first few weeks (Fig. S2 in the Supplement). Flagellates between 3 and 6 µm included cells resembling Mamiellales (Fig. S3). Mixotrophic cryptophytes accounted for a small fraction of the autotrophic biomass (Fig. 4). The coccolithophore *Emiliania huxleyi* declined inside but also outside the patch from 0.48 g C m^{-2} on Day −1 to 0.14 g C m^{-2} at the end of the experiment (Figs. 4 & 6).

Total autotrophic dinoflagellates, detected with confidence in formalin-fixed samples by their chloroplasts under epifluorescence, nearly tripled their biomass inside the patch from Day −1 (0.46 g C m^{-2}) to Day 33 (1.2 g C m^{-2}) (Fig. 4). Biomass of dinoflagellates <20 µm was dominated by unarmoured taxa and remained fairly stable (average 0.33 ± 0.08 g C m^{-2}). The increase in biomass from Day 9.5 onwards was mostly due to the intermediate 20–40 µm size class (Fig. 5). The biomass of autotrophic dinoflagellates also increased outside the patch but to a lesser extent, from 0.52 on Day −1 to 1.0 g C m^{-2} at the end of the experiment (Fig. 4).

The diatom contribution to PPC was minor (~5%; Figs. 4 & 5) with 10 taxa, generally comprising cells at the lower end of their respective size ranges, accounting for 95% of the total biomass. These were: *Corethron pennatum*, *Ephemera* sp., *Fragilariopsis*

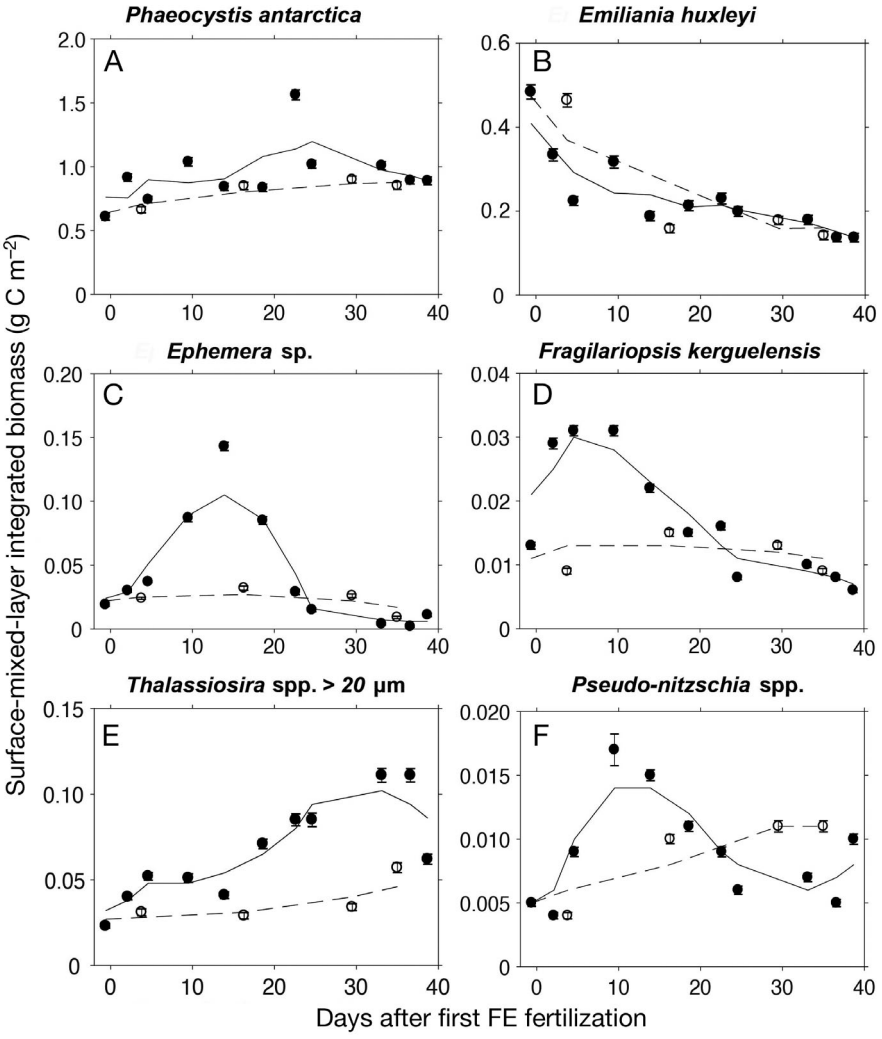

Fig. 6. Time courses of the biomass stocks integrated for the 80 m surface mixed layer in g C m^{-2} of (A) solitary *Phaeocystis* cells, (B) *Emiliania huxleyi*, (C) *Ephemera* spp., (D) *Fragilariopsis kerguelensis*, (E) *Thalassiosira* spp. >20 µm and (F) *Pseudonitzschia* spp. inside (filled circles) and outside the iron-fertilized patch (open circles) (see Fig. 1), showing differences in, or lack of, response to iron fertilization

kerguelensis, *Haslea trompii*, *Lennoxia flaveolata*, *Navicula* sp., *Pseudo-nitzschia* spp., *Thalassionema nitzschioides* and *Thalassiosira* spp. <20 and >20 µm. Total diatom biomass did not change much during the experiment (Fig. 5), from initial, peak and final values of 0.42, 0.49 and 0.37 g C m^{-2}, respectively. Values were lower outside the patch. There were marked differences in the response patterns of the above species. Thus, stocks of *Ephemera* sp., *F. kerguelensis* and *Pseudo-nitzschia* spp. initially increased 7.5-, 2.4- and 3.4-fold until Days 14, 9 and 9, respectively, while stocks outside stayed rather constant in the former 2 species and increased 2-fold in the latter species (Fig. 6). The population of *C. pennatum* remained stable throughout, whereas *Thalassiosira* spp. in the size classes <20 and >20 µm increased their biomass steadily, reaching 0.19 and 0.12 g C m^{-2} inside and outside, respectively (Fig. 6).

Distances/similarities of phytoplankton assemblages between stations

In order to compare the phytoplankton assemblage between different stations inside the patch, we calculated the Hellinger distance D (Legendre & Legendre 2012) and divided it by $\sqrt{2}$. The resulting scaled Hellinger distance D_s can vary between 0 and 1. The corresponding similarity index $S_H = 1 - D_s$ can vary between 1 and 0. The similarity indices calculated for all stations inside the patch were quite high (Table 1), indicating no major changes in the phytoplankton assemblage over time after iron fertilization. The number of stations outside the patch were insufficient for the analysis but their assemblages did not noticeably differ from those inside the patch.

Protozooplankton

Protozooplankton carbon (PZC), which includes all obligate heterotrophic protists, remained relatively stable and averaged 1.8 ± 0.23 g C m^{-2} inside and 1.8 ± 0.22 g C m^{-2} outside the patch (Fig. 7). On average, heterotrophic nanoflagellates (including choanoflagellates but excluding dinoflagellates <20 µm) contributed 0.57 ± 0.15 g C m^{-2}, aloricate ciliates 0.73 ± 0.15 g C m^{-2}, and all heterotrophic dinoflagellates 0.49 ± 0.13 g C m^{-2} inside the patch (Fig. 5); these values corresponded to 30.5 ± 5.7, 40.1 ± 7.4 and 26.4 ± 7% of the total PZC biomass, respectively. The remainder, 0.062 ± 0.015 g C m^{-2}, was contributed by Rhizaria (Acantharia, Radiolaria, Foraminifera and Heliozoa). The biomass of copepod larvae (nauplii and early copepodite stages) assessed in the 12 l samples is included in Fig. 7. Their contribution averaged 0.27 ± 0.06 g C m^{-2} inside and 0.26 ± 0.02 g C m^{-2} outside the patch.

Table 1. Similarity indices (S_H) for phytoplankton assemblages inside the iron-fertilized patch based on scaled Hellinger distance D_s. Days correspond to time after fertilization. Only stations where data on larger protists and copepods were available (see 'Results' for explanation) were considered for the analysis. Stn 114 was visited directly before fertilization

Day	Stn no.	114	132	135	139	162	192
4.6	132	0.83					
9.5	135	0.87	0.91				
13.9	139	0.83	0.91	0.95			
24.6	162	0.83	0.87	0.94	0.93		
33.1	192	0.84	0.86	0.91	0.9	0.89	
36.6	204	0.83	0.88	0.91	0.91	0.89	0.97

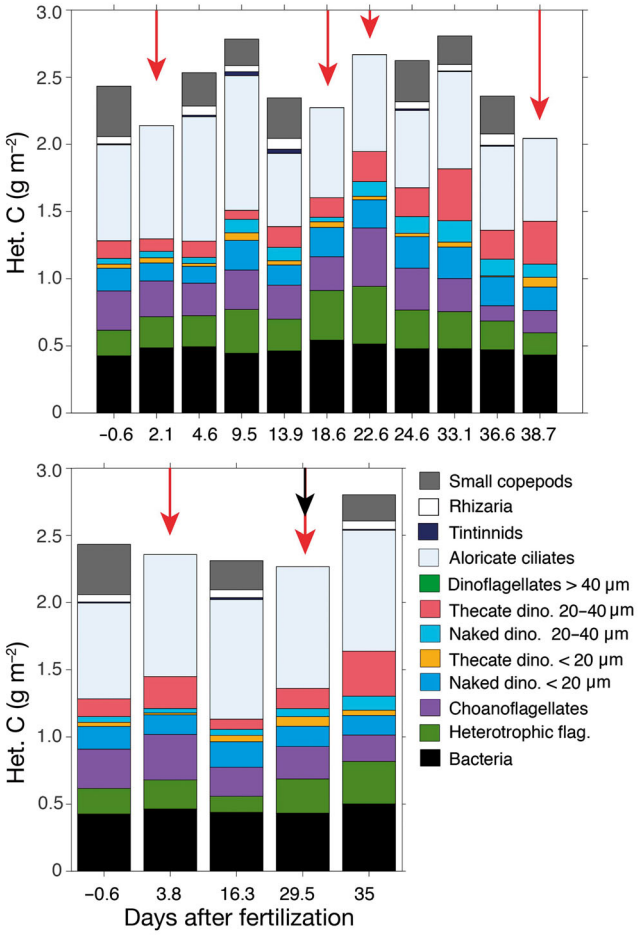

Fig. 7. Total carbon of heterotrophs <1 mm from (A) inside and (B) outside the iron-fertilized patch (see Fig. 1) including bacteria, heterotrophic nanoflagellates (Heterotrophic flag.), choanoflagellates, unarmoured dinoflagellates (Naked dino. <20 µm), thecate dinoflagellates (Thecate dino. <20 µm), unarmoured dinoflagellates (Naked dino 20–40 µm), thecate dinoflagellates (Thecate dino. 20–40 µm), dinoflagellates >40 µm, aloricate ciliates, tintinnids and Rhizaria (comprising Foraminifera, Acantharia and Radiolaria), small copepods (<1 mm, including nauplii and small copepodites). The latter 3 categories were counted in 12 l concentrated samples that were not taken at the stations marked with the red arrows. The black arrow indicates the edge station

The organisms grouped under heterotrophic nanoflagellate (HNF) biomass include all small flagellates without chloroplasts; most were unidentified, but some recognizable taxa such as *Leucocryptos marina*, *Plagioselmis* sp. and *Telonema* sp. were recorded. Choanoflagellates were also differentiated. Inside the patch, HNF biomass exhibited a distinct, albeit small, increasing trend until Day 22 that was not evident outside the patch. Interestingly, choanoflagellates contributed about half of the total HNF biomass throughout. Heterotrophic dinoflagellates almost doubled biomass from 0.37 to 0.82 g C m^{-2} (0.17 to 0.55 g C m^{-2} for the fraction >20 µm) from the beginning to the end of LOHAFEX inside the patch, with a steady increasing trend throughout the experiment (Figs. 5 & 7). The increase was due to thecate and athecate groups in the size category 20–40 µm; a lesser increase also occurred in outside water.

Total ciliate biomass inside the patch was slightly higher than that of dinoflagellates and increased steadily from 0.72 to 1.03 g C m^{-2} until Day 9.5 but declined thereafter (Fig. 5). The increase was due to the size class 40–90 µm, although the bulk of ciliate biomass (average 71 ± 9.7 %) was present in the size class <40 µm. Tintinnids were represented only by small species (such as *Acanthostomella norvegica*, *Codonellopsis pusilla* and *Cymatocylis antarctica*), with the characteristic large species of the ACC notably rare or absent, and accounted for only ~2 % of the ciliate biomass. The ratio of full to empty and damaged tintinnid loricae, a measure of grazing pressure (Assmy et al. 2014), was similar throughout. Ciliate biomass and composition did not differ significantly inside and outside the patch (Fig. 5). Biomass of Rhizaria was remarkably low throughout the experiment and ranged between 0.05 and 0.08 g C m^{-2}.

DISCUSSION

The LOHAFEX experiment in relation to its surroundings

The most productive region of the ACC is the SW Atlantic sector due to its multiple sources of iron. South Georgia is a major source, evidenced by the plume of enhanced chlorophyll concentrations extending eastward along the Polar Front that was also present in the late summer of 2009 (Fig. 1). The cold core of the eddy in which the LOHAFEX experiment was conducted emanated from the tail end of this plume and had much higher chlorophyll concentrations than the adjacent warm core (anticyclonic)

eddy, containing impoverished water from north of the Antarctic Polar Front (Fig. 1). The peak chlorophyll concentration attained by the bloom was not captured by the satellite due to cloud cover, but it would have been in the same range as the blooms northeast of South Georgia.

Satellite images of chlorophyll distribution show surface concentrations and not water column stocks. In the characteristic deep mixed layers of the Southern Ocean (60–100 m) chlorophyll concentrations >1 mg chl *a* m^{-3} qualify for bloom status as their integrated water column stocks are equivalent to those of blooms with 3- to 4-fold higher concentrations, albeit in shallower mixed layers characteristic of other productive ocean regions. The satellite image shows that within 2 wk, the LOHAFEX bloom had attained the medium range of the patches and streaks of enhanced chlorophyll concentrations (>1 mg chl *a* m^{-3}) surrounding it (Fig. 1). It follows that the most likely cause of these patchy and frontal blooms is local iron input, the source of which could be dust outfall (Cassar et al. 2007, Boyd et al. 2012) but also the many melting icebergs (Raiswell et al. 2008, Wu & Hou 2017) we encountered in the region, some of which were very large (Smetacek & Naqvi 2010). Since the pre-experimental survey made to the longitude of South Georgia (Smetacek & Naqvi 2010) found extremely low silicate concentrations (<3 mmol Si m^{-3}) and low diatom abundances in the entire region, it is highly unlikely that, in this late season, diatoms contributed significantly to the biomass of these natural blooms.

The phytoplankton of the LOHAFEX region was clearly iron-limited, as indicated by the increase in maximum quantum yield (F_v/F_m) following fertilization, which rose from 0.33 to a maximum of 0.5 on Day 14 (Martin et al. 2013). Alleviation of iron limitation was also reflected in the decline in POC:chl *a* ratios (from ~200 to ~140) during the first 10 d (Fig. 2) apparently due to an increase in cellular chlorophyll that is characteristic of phytoplankton relieved of iron limitation (Landry et al. 2000a, Boyd et al. 2007). Thereafter, ratios stabilized, suggestive of a saturation state because chlorophyll stocks continued increasing steadily inside the patch (Fig. 2) from 40 to 90 mg chl *a* m^{-2} reached on Day 22. Stocks then decreased at first fairly abruptly and levelled off at values significantly above outside values, which remained more or less constant throughout the experiment (Fig. 2).

The first abrupt decline in chl *a* and POC stocks between Days 22 and 24 was primarily due to dilution with outside water, as it occurred concomitantly with the elongation and rapid movement of the patch within the collapsing eddy (Martin et al. 2013). Thereafter, the patch consolidated, dilution rates decreased, and chlorophyll concentrations stabilized. The biomass decline was not due to sudden, mass sinking, as transmissometer profiles showed no increase in spikes that would have signalled aggregate formation (Briggs et al. 2011), nor did particle concentrations increase in subsurface layers as observed during the mass sinking event that occurred in the diatom bloom of the EIFEX experiment (Smetacek et al. 2012). Catches of neutrally buoyant sediment traps and thorium losses corroborated this conclusion (Martin et al. 2013). It needs to be pointed out that, despite dilution, patch waters differed significantly from the unfertilized surroundings throughout the experiment in terms of their consistently lower POC:chl *a* ratios (Fig. 2). Correlations between discrete concentrations of POC and chl *a* inside and outside the patch were highly significant in each case, with strongly differing slopes of 110 and 157. This suggests that iron availability inside the patch was higher than in the surroundings, enabling iron-limited phytoplankton, mixed in with patch water during dilution, to rapidly respond by increasing F_v/F_m and cellular chlorophyll concentrations.

The effects of dilution were reflected in POC and chlorophyll stocks, but to a much lesser extent in protist community composition because of the similarity inside and outside the patch (Figs. 2 & 3). Because of patch movement in relation to surrounding water, the outside stations sampled different water masses, so the fact that there were only minor differences between them indicates that horizontal homogeneity in ecosystem structure prevailed at a regional scale. Given the regional homogeneity indicated by the outside stations, it is likely that the composition of the LOHAFEX bloom was basically similar to those of the natural blooms surrounding it (Fig. 1) and can be considered representative of the region of the iron-enriched, silicate-limited Antarctic Zone water mass extending westward to the longitude of South Georgia (Fig. 1).

Composition of plankton biomass

By far, the bulk of plankton biomass was located in the nanoflagellate size classes 3–6 and 6–20 µm, with the smallest size class including picoplankton (<3 µm) playing a negligible role. The percentage contribution of these 3 size classes to their combined biomass both inside and outside the patch was remarkably

similar throughout the experiment (<3 µm: 3.7 ± 2.4 %; 3–6 µm: 63.8 ± 5.8 %; >6 µm: 32.5 ± 6.1 %), suggesting that they were equally affected by the balance between growth and mortality. We combined the 3 size classes and refer to them as autotrophic nanoflagellates (ANF) in the following but point out that the bulk of the biomass was centred around 5 µm. It should be mentioned here that the 10 % overestimation of the total unicellular PC vs. POC is presumably located in the ANF; however, even if we deduct 20 % (to also account for detritus particles that might have been inadvertently counted as coccoid cells) from ANF biomass, the error is small and does not weaken the main conclusions drawn here on quantitative relationships between the ecosystem components. The same applies to a possible overestimation of ANF by inadvertent inclusion of obligate HNF in the counts.

The biomass increment of 4.3 g C m^{-2} by the ANF over 3 wk is surprisingly high and in the same range as the total diatom biomass built up during the first 3 wk of the spring and late-summer OIF experiments EisenEx and EIFEX: 3.2 and 3.8 g C m^{-2}, respectively (Assmy et al. 2007, 2013). The difference between the diatom and ANF blooms lies in the magnitude of the peak chlorophyll stocks, which were much greater: 231 and 286 mg chl *a* m^{-2} in EisenEx and EIFEX respectively, versus 90 mg chl *a* m^{-2} for LOHAFEX. The low C:chl *a* ratios of nutrient-replete diatoms can be explained by considering the ratio of the biovolume of chloroplasts relative to other organelles that have the same carbon:volume ratio but lack chlorophyll. In diatoms, chloroplasts are conspicuous under the microscope and contribute by far the bulk of their visible biomass (plasma carbon) because nuclei and other organelles are relatively small. In species with large vacuoles, chloroplasts adhere as a single layer to the inside of the frustule wall, with most of the vacuole volume occupied by water. The size and/or density of chloroplasts increase visibly following addition of the limiting nutrient, whether N or Fe. In ANF, on the other hand, chloroplasts, although often relatively large, do not generally occupy the entire visible cell volume; vacuoles are small but nuclei and other organelles tend to occupy relatively more cellular space than in diatoms. Besides, many species possess large flagella relative to cell size (Fig. S3), or invest in robust organic cell walls, and others are covered with organic scales or thecae. All of these properties evolved as alternative defence mechanisms against various types of pathogens and grazers in the evolutionary arms race in which the diatom silica frustule proved itself to be particularly effective (Hamm & Smetacek 2007). Besides, most autotrophic flagellates are also capable of heterotrophy, which will require dedicated organelles for ingestion and digestion of particles (Stoecker et al. 2017). All of these extra organelles packed into the ANF cells can be expected to increase the C:chl *a* ratio of ANF relative to diatoms. It follows that biomass of ANF-dominated blooms will be underestimated if the same C:chl *a* ratios are used to interpret satellite images of chl *a* distribution (Finenko et al. 2003, Sathyendranath et al. 2009).

It is worth briefly comparing the photosynthetic performance of the ANF community with that of the diatoms because the former built up comparable biomass at similar daily rates of primary production but with one-third the chlorophyll (Gervais et al. 2002, Smetacek et al. 2012, Martin et al. 2013). In both EisenEx and EIFEX blooms, nitrate uptake was stimulated by iron fertilization but not during LOHAFEX, as there was negligible difference to outside waters. This observation is noteworthy because both chlorophyll synthesis and nitrate reduction have an obligate iron requirement. It is likely that mixotrophy amongst the ANF was responsible for stability of their biomass composition (Flynn et al. 2013).

Role of heterotrophy in ANF

Many of the mixotrophic flagellates, together with the 'classic' bacterivorous HNF (Fenchel 1987, Stoecker et al. 2017), will have ingested bacteria. A detailed study of bacterial production rates, abundance and biomass as well as taxonomic composition revealed higher thymidine and leucine uptake rates inside the patch but otherwise only minor differences in abundance, biomass and taxonomic composition between inside and outside the patch (Thiele et al. 2012). A remarkable feature of the bacterial assemblage was the absence of trends over time in biomass and composition both inside and outside the patch. Bacterial biomass remained stable and contributed only 6 and 5.5 % to total unicellular plankton biomass at inside and outside stations, respectively. The rather low biomass levels were attributed to the heavy grazing pressure exerted by the order of magnitude larger biomass of the potentially bacterivorous flagellate assemblage. Indeed, the only significant, albeit minor, increase in any of the bacterial taxa was the clade SAR11, which is reputed to be protected from grazers by its small size (Thiele et al. 2012).

Bacteria are considered to be a key component of recycling systems; however, given the low bacterial

biomass compared to the 10-fold higher ANF, it appears unlikely that bacterial production, estimated at about 1 division d^{-1} from thymidine uptake rates (Thiele et al. 2012), could have satisfied even a fraction of the potential demand of the mixotrophs. Indeed, the biomass of specialized bacterivorous HNFs, with similar or even higher growth rates (Eccleston-Parry & Leadbeater 1994), was already in the same range or higher than that of bacteria (Fig. 7). Since by far the bulk of total biomass, hence also biogenic iron, was in the ANF fraction, it is reasonable to assume that nutrient regeneration and iron recycling was occurring within it (Sherr & Sherr 2002). For instance, it is possible that detritus particles e.g. emanating from the breakdown of copepod faeces, were ingested by mixotrophic ANF. This would explain the paucity of visible detritus particles in the samples and the prolonged availability of iron within the patch (Laglera et al. 2017). Such a recycling pathway would provide a stabilizing link within the ANF community augmented by grazing of ANF by microplanktonic protozooplankton.

Particle ingestion has 2 advantages for a mixotroph: it provides food for the phagotrophic part of the cell — the exosymbiont — and the breakdown products provide nutrients to the chloroplasts — the endosymbiont (Smetacek 2012, Ward & Follows 2016). Mixotrophs with the ability to also take up dissolved inorganic nutrients would then be the most efficient biomass builders, so it is a valid question to ask why diatoms and the colonial stages of *Phaeocystis*, that are incapable of phagotrophy, tend to dominate blooms throughout the oceans. The answer most probably lies on the other side of the balance regulating biomass build-up: mortality by the '3 Ps': predators, parasitoids and pathogens (Smetacek 2012). Thus, the totally-encasing diatom frustule and *Phaeocystis* colony skin (Hamm et al. 1999) provide an effective barrier to viral and peduncle attack, to which phagotrophs are exposed via their vulnerable opening during particle ingestion. Unfortunately, we have no information on mortality within the ANF community but, since they overwhelmingly dominated total biomass throughout, their stability and resistance point to internal controls, i.e. grazing and recycling within the community. The high gross growth efficiency normalized to chlorophyll of the ANF versus diatom blooms (~20 compared to ~5 mg C mg^{-1} chl *a* d^{-1}, respectively) could partly be explained by a contribution of heterotrophy to biomass build up (Ward & Follows 2016, Stoecker et al. 2017). Given the broad range of feeding types evolved by dinoflagellates (Jacobson 1999), it is likely that predation, i.e. active capture of equal-sized or smaller prey, has also evolved in other nanoflagellate groups and could be worthwhile looking for.

Evidence for species succession from the identified nanoflagellate populations is equivocal (see also Thiele et al. 2014). Thus, solitary cells of *Phaeocystis* maintained stable populations throughout with no difference between inside and outside the patch, whereas *Emiliania huxleyi* declined 2-fold at similar rates but for unknown reasons both inside and outside (Fig. 6). Since only armoured cells were counted, it is possible that a transition to an unarmoured stage in their complex life cycle was responsible (Frada et al. 2012). Flagellates belonging to the Mamiellales (3–6 µm), on the other hand, followed the general ANF trend.

Interestingly, the biomass of heterotrophic dinoflagellates <20 µm and HNF, to which choanoflagellates contributed about half, followed the same pattern as the major fraction of ANF: a steady increase until doubling in the first 3 wk followed by declining stocks inside the patch. Although biomass stocks of HNF were roughly an order of magnitude lower than ANF, the similarity is striking and suggests a common cause for biomass buildup and maintenance by both phyto- and protozooplankton taxa within this size class.

In contrast, during the EIFEX diatom bloom, the biomass of non-diatom phytoplankton including nanoflagellates remained stable throughout the 5 wk experiment at 0.82 ± 0.13 g C m^{-2} inside the patch and 0.63 ± 0.22 g C m^{-2} outside it without clear signs of a response to iron alleviation (Assmy et al. 2013). Similarly, biomass of HNF at 0.04 ± 0.005 g C m^{-2} was only 3.1 ± 0.5% of total heterotrophic biomass. Given that the physico-chemical environment (light and nutrient supply except for silicate) was similar in both experiments, it is unlikely that bottom-up factors were at play in controlling the ANF during EIFEX. The same situation also applied to the EisenEx experiment where biomass of all non-diatom phytoplankton (mostly ANF) also remained fairly stable at 0.61 ± 0.21 and 0.48 ± 0.10 g C m^{-2} inside and outside the patch, respectively (Assmy et al. 2007). Why grazing pressure on nanoflagellates was so much higher in the diatom blooms is obscure: ciliate and heterotrophic dinoflagellate stocks were somewhat lower during EIFEX, although total protozooplankton biomass was in the same range due to the large acantharian stocks (Assmy et al. 2014). At this stage of our knowledge, we cannot rule out other factors such as allelopathy, e.g. by diatoms (Xu et al. 2015), but the much-invoked nutrient competition amongst phyto-

plankton functional groups, at least in the early stages of the experiments when nutrients were sufficient, appears to be unlikely. Another widely held belief, that diatoms are favoured over flagellates in turbulent waters, can also be ruled out as wind speeds and storm frequency did not differ between the experiments. The only difference in physicochemical regimes was the availability of silicate for net diatom growth; the rest has to be biology.

The well-known grazers of nanoflagellates are ciliates and possibly some dinoflagellates; however, given their relatively low biomass levels it is unlikely that their predation pressure imposed a significant constraint on the ANF stock size. The fact that microprotozooplankton stocks in general were remarkably stable suggests that their biomasses were also controlled by grazers, which would be the 3 dominant species of copepods present in the region: the small *Oithona similis*, medium-sized *Ctenocalanus citer* and the large *Calanus simillimus*. The latter dominated copepod biomass by far (Mazzochi et al. 2009). One could assume that the dominant ANF size class was below the handling ability of these copepods. Salps, major nanoflagellate grazers particularly abundant in the Southern Ocean (Smetacek et al. 2004), were rare or absent in midwater trawl catches throughout the LOHAFEX cruise, although the few individuals caught were in an active growth stage (H. Gonzales unpubl. data). Since they have very high growth rates, their near absence during LOHAFEX points to heavy predation pressure exerted by the predatory amphipod *Themisto gaudichaudii*, the only zooplanktivore present in large numbers in the region (Mazzochi et al. 2009). Thus, the well-documented control on protozooplankton biomass by copepods (Irigoien et al. 2005, Sherr & Sherr 2009), coupled with the veritable absence of salps due to predation by *T. gaudichaudii*, could well be the major factors responsible for creating the 'loophole' in the otherwise tightly geared food web within which the ANF built up their bloom.

Microphytoplankton response to alleviation of iron limitation

Microphytoplankton biomass (comprising cells >20 µm belonging to diatoms, silicoflagellates, *Phaeocystis* colonies, autotrophic dinoflagellates), with an average value of 0.90 ± 0.24 SD g C m^{-2} inside the patch and 0.7 ± 0.2 g C m^{-2} outside the patch was less then 15% of total phytoplankton biomass with autotrophic dinoflagellates >20 µm and diatoms contributing 6.4 ± 2.7% and 5.7 ± 2.2% inside the patch, and 5.8 ± 1.8% and 5.5 ± 1.6% outside the patch, respectively. The dinoflagellates included species such as *Prorocentrum* cf. *balticum* and *Tripos* (=*Ceratium*) *pentagonus* belonging to widely distributed genera that frequently form blooms in coastal regions (Assmy & Smetacek 2009). It is of interest to note that this group responded to iron fertilization by increasing biomass 3-fold. An increase outside the patch was also noticeable and could be attributed to the autumn upsurge in dinoflagellates characteristic of high latitudes. Observations of dinoflagellate thecae including *Tripos* (=*Ceratium*) in copepod faeces suggest that the group as a whole was heavily grazed by copepods. We also attribute the near absence of *Phaeocystis* colonies to heavy grazing on the early stages of colony formation.

Despite extremely low silicate concentrations, the total diatom stock increased slightly inside the patch, significantly above outside values where little change occurred. The strongest response to iron fertilization was the weakly silicified, pennate diatom *Ephemera* sp. that increased biomass 7-fold within the first 2 wk to about 30% of total diatom biomass but crashed in the third week and reached vanishingly low concentrations at the end (Fig. 6). This expression of a boom-and-bust strategy in a diatom population at such low silicate concentrations is noteworthy, as it indicates that species life cycles can also be completed at silicate levels considered to be limiting (Egge & Aksnes 1992). This behaviour has also been observed in diatoms from the subtropical gyre off Hawaii (Scharek et al. 1999).

Also noteworthy is the behaviour of the heavily and weakly silicified pennate diatoms *Fragilariopsis kerguelensis* and *Pseudo-nitzschia* sp., respectively, that doubled biomass in the first 2 wk (Fig. 6). The first species plays a key role in the global silicon cycle (Assmy et al. 2006, 2013), and some species of the cosmopolitan genus *Pseudo-nitzschia* are considered harmful to higher trophic levels (Trainer et al. 2012). The factors that led to both species returning to initial values in the second half of the experiment could have been due to grazing (Fig. 6). During the EisenEx and EIFEX blooms, *F. kerguelensis* exhibited a similar response pattern, albeit at 30-fold higher biomass levels (Assmy et al. 2007, 2013). In contrast, species of the centric genus *Thalassiosira* (in the size categories <20 and >20 µm) steadily increased biomass to 4-fold the initial value inside the patch to reach 50% of diatom biomass (Fig. 6). The same species group also increased steadily outside but to only 2-fold higher values, suggesting that the population size of this

robust cell-walled genus was regulated more by iron availability than by silicate.

The dynamics exhibited by some diatom populations can be explained by comparing the silicon inventory of living diatom frustules with the dissolved pool. Thus, the average diatom stock size of 0.4 g C m^{-2} (33 mmol C m^{-2}) assuming a C:Si ratio of 6 (ocean average) or 3 (Southern Ocean average) ranged between 6 and 11 mmol Si m^{-2} and was far below the minimum and average in-station 80 m integrated silicate stock of 42 mmol Si m^{-2} and 84 ± 31 SD mmol Si m^{-2}, respectively, indicating that limited biomass build up and population fluctuation within the diatom pool was possible despite the low silicate concentrations. The role of empty and crushed frustules in silicon recycling within the mixed layer is unknown but is likely not insignificant. The observations indicate that many diatoms, including heavily silicified species, can increase their populations at silicate concentrations well below the 3 mmol Si m^{-3}, long believed to be growth-limiting for diatom uptake (Egge & Aksnes 1992). Our observations indicate that species succession within the diatom assemblage also occurs at very low silicate concentrations.

Protozooplankton

PZC comprising HNF, dinoflagellates and ciliates in roughly equal proportions was remarkably stable throughout the experiment and ranged around 18% of protistan biomass inside and outside the patch. Only the thecate dinoflagellates >20 µm showed an increasing trend during the 40 d, which was compensated by the aforementioned HNF decline after Day 22. Ciliates did not show a marked or lasting response to fertilization, despite the apparent abundance of potential food. Indeed, their stocks remained remarkably stable (0.7 ± 0.2 and 0.9 ± 0.1 g C m^{-2}) both inside and outside. Large tintinnids, normally a prominent feature of the ACC, were surprisingly rare, and even the ubiquitous small species were unusually scarce. As mentioned above, ciliates are known to be specialized feeders of nanoflagellates, but they are choosy feeders and ingest only selected prey items. Their feeding behaviour is likely to have had an effect on ANF composition but more cannot be said at this stage of our knowledge. Much less is known about the species-specific feeding behaviour of dinoflagellates vis-à-vis nanoflagellates, but they are known to have evolved a broad range of feeding techniques that allow them to prey on equal or larger sized cells including diatoms and ciliates (Jacobson 1999). Whereas ciliate and dinoflagellate biomasses were in the same range as in EisenEx and EIFEX, the HNF were at much higher levels. We suggest that had copepod grazing pressure been substantially lower during LOHAFEX, it would have allowed ciliates and dinoflagellates to proliferate and graze down the nanoflagellates. Such events have been observed in mesocosms incubated with natural water (Smetacek 1984).

A noteworthy feature of the LOHAFEX community was the near-absence of Rhizaria. Acantharia responded to fertilization by roughly doubling in biomass during Eisenex (Henjes et al. 2007b) and EIFEX (Assmy et al. 2014), where their biomass was higher than that of ciliates and dinoflagellates. It was argued that this group was defended against smaller ingesting grazers by their robust spines, similar to the persistent, thick-shelled diatom species that contributed to the bloom. However, given the low microplankton biomass in LOHAFEX, copepods were likely to have been less selective in their feeding behaviour and also fed on Acantharia. Circumstantial evidence for the heavy grazing pressure exerted by the copepod populations on microplankton was obtained from routine observations of live plankton and copepod faecal pellets collected with a 20 µm mesh hand-net at the start of each station (Figs. S4 & S5 in the Supplement). During the course of the experiment, a distinct decline in abundance and species diversity of large protists was observed, and towards the end of the experiment, only Foraminifera were conspicuous. These were species with and without spines and about half with chl *a*-bearing symbionts. Instances where the spines had been bitten off or where bundles of bitten-off spines or crushed foraminifera shells were found in copepod faecal pellets (Fig. S5) indicated that the copepods are likely to have been food limited.

Implications for carbon cycling

Nanoflagellate-dominated pelagic ecosystems (low-latitude *E. huxleyi* blooms excepted) are characteristic of nutrient-depleted surface layers and, as explained in the Introduction, generally occur at biomass levels substantially lower than those of the preceding blooms of microphytoplankton responsible for the nutrient depletion. The situation in the SW Atlantic region encountered during LOHAFEX indicates that ANF-dominated communities cannot only exist, but also persist at biomass levels rivalling those of microphytoplankton blooms. However, in contrast to

diatom blooms whose biomass has been observed to sink out of the surface layer (Smetacek 1998) and arrive at the deep-sea floor within weeks (Lampitt 1985, Smetacek et al. 2012), vertical flux from the ANF bloom was modest and shallow (Martin et al. 2013). Further, there was no difference between the magnitude of vertical flux from inside and outside the patch, indicating that loss rates were not necessarily a function of the primary production and biomass in the surface layer (Martin et al. 2013). This was indicated by the transmissometer profiles, the catches of neutrally buoyant traps and thorium deficit measurements (Martin et al. 2013). The latter indicated loss rates of 0.075 g C m^{-2} d^{-1}, which amounts to about 30% of net community production estimated with O_2:Ar ratios (Martin et al. 2013). Over a 38 d period, this would add up to 2.8 g C m^{-2} or about 25 and 30% of the peak POC stocks inside and outside the patch, respectively.

The LOHAFEX community can best be described as largely a regenerating community in which a steady but small supply of new nitrogen compensated equivalent losses due to sinking. Nitrate uptake rates inside and outside the eddy were much the same, implying that iron sufficiency did not increase the synthesis of nitrate reductase as was the case in chlorophyll. In short, CO_2, but not nitrate uptake, was stimulated by iron amendment. We conclude that mainly the photosynthesis machinery of the regenerating community responded to iron fertilization by increasing cellular chlorophyll levels.

In contrast to the rapidly sinking aggregates from diatom blooms, the flux from the ANF bloom comprised smaller, hence slower-sinking particles that were used by heterotrophs within the upper few 100 m (Martin et al. 2013). Despite the large numbers produced in the surface layer, only few copepod pellets were collected in neutrally buoyant sediment traps deployed at 200 and 400 m depths (Ebersbach et al. 2014, M. Iversen & H. Gonzales unpubl. data). The ANF bloom was most probably terminated later in the year by the onset of winter cooling and convective vertical mixing of surface with subsurface layers leading to formation of the deep mixed winter layer and dilution of bloom biomass. Upward mixing of the subsurface layer would return a significant proportion of CO_2 released by the shallow export flux from non-diatom blooms to the atmosphere. It follows that ANF-dominated blooms are likely to play a minor role in long-term carbon sequestration.

Biogeochemical models of the carbon cycle based on satellite-derived chlorophyll imagery will have to take account of the differing impacts of late summer blooms in silicate-depleted water of the SW Atlantic sector but also in the entire Southern Ocean north of the Antarctic Polar Front from those of spring blooms and summer blooms in the Antarctic Zone south of it. However, it must be remembered that heavy predation pressure on microphytoplankton but also microprotozooplankton grazers of ANF by the large copepod population — a characteristic feature of the entire ACC (Smetacek et al. 2004) — is the most likely reason for the ANF dominance we encountered. The relative absence of salps is another precondition for ANF bloom build up. Their role in carbon sequestration is not yet quantified, and there is little direct evidence for the hypothesis that salp faecal pellets are fast-sinking and reach substantial depths (Richardson & Jackson 2007, Iversen et al. 2017). Thus, although salp abundances can be substantial, their role in carbon sequestration, whether as cadavers or pellets, needs dedicated study.

Concluding remarks

The LOHAFEX bloom demonstrates that ANF can, under conditions of silicate limitation, build up biomass stocks rivaling those of diatoms and maintain the high biomass levels over long periods. Apart from their implications for biogeochemistry (Martin et al. 2013), the LOHAFEX results also shed light on ecosystem structure and functioning as they indicate that a dynamic equilibrium can be maintained over periods of many weeks by organisms with fast division rates (Weisse & Scheffel-Möser 1990, Giovannoni & Vergin 2012). Thus the comparatively modest impact of experimental alleviation of a limiting resource showcases the potential stability of a microbial network of tight interactions between bacteria and a phylogenetically diverse assemblage of nanoflagellates comprising obligate heterotrophic, mixotrophic and possibly obligate autotrophic species (Strom 2008). Apparently, feedback loops within the network buffered the effects of perturbation by nutrient addition and stabilized its structure.

The pelagic community encountered during LOHA FEX represented a late or probably final stage in seasonal succession of the pelagic community, eventually terminated by winter convection. Its resistance to perturbation could be related to the fact that the trophic interactions between the relevant components maintaining the system had evolved over the prior months and as a result had matured into a stable state. We attribute the absence of population

build-up by larger bloom-forming species other than diatoms such as *Phaeocystis* colonies or dinoflagellates, to selective grazing exerted by copepods on their developmental stages and potential seed stocks, respectively. A possible explanation for why non-diatom microphytoplankton blooms are 'nipped in the bud' in the silicate-limited ACC but not elsewhere is provided by the 'merry-go-round' hypothesis of the ACC ecosystems enabling long residence time of the water masses comprising the zonal branches of the ACC within much the same climate zone (Smetacek et al. 2004). Stability of the physical environment should promote selection of organism interactions with stabilizing feed-backs that are maintained over large regional scales.

Acknowledgements. We are indebted to the captain and crew of RV 'Polarstern' and the scientific team of LOHAFEX. The Council of Scientific and Industrial Research (CSIR), India and the Helmholtz Foundation, Germany, equally shared the costs of the experiment. This work was funded through the DFG Research Center / Cluster of Excellence 'The Ocean in the Earth System'. I.S. was supported by GLOMAR Bremen International Graduate School for Marine Sciences. We thank Diana Sarno and Adriana Zingone (Stazione Zoologica Anton Dohrn, Napoli, Italy) for SEM preparations and support in taxonomical identification.

LITERATURE CITED

Abelmann A, Gersonde R, Cortese G, Kuhn G, Smetacek V (2006) Extensive phytoplankton blooms in the Atlantic sector of the glacial Southern Ocean. Paleoceanography 21:PA1013

Assmy P, Smetacek V (2009) Algal blooms. In: Schaechter M (ed) Encyclopedia of microbiology. Elsevier, Oxford, p 27–41

Assmy P, Henjes J, Smetacek V, Montresor M (2006) Auxospore formation by the silica-sinking, oceanic diatom *Fragilariopsis kerguelensis* (Bacillariophyceae). J Phycol 42:1002–1006

Assmy P, Henjes J, Klaas C, Smetacek V (2007) Mechanisms determining species dominance in a phytoplankton bloom induced by the iron fertilization experiment EisenEx in the Southern Ocean. Deep Sea Res I 54:340–362

Assmy P, Smetacek V, Montresor M, Klaas C and others (2013) Thick-shelled, grazer-protected diatoms decouple ocean carbon and silicon cycles in the iron-limited Antarctic Circumpolar Current. Proc Natl Acad Sci USA 110:20633–20638

Assmy P, Cisewski B, Henjes J, Klaas C, Montresor M, Smetacek V (2014) Response of the protozooplankton assemblage during the European Iron Fertilization Experiment (EIFEX) in the Antarctic circumpolar current. J Plankton Res 36:1175–1189

Beers JR, Stewart GL (1970) The preservation of acantharians in fixed plankton samples. Limnol Oceanogr 15: 825–827

Bishop JKB (1999) Transmissometer measurement of POC. Deep-Sea Res 46:353–369

Borrione I, Aumont O, Nielsdóttir MC, Schlitzer R (2014) Sedimentary and atmospheric sources of iron around South Georgia, Southern Ocean: a modelling perspective. Biogeosciences 11:1981–2001

Boyd PW, Jickells T, Law CS, Blain S and others (2007) Mesoscale iron enrichment experiments 1993-2005: synthesis and future directions. Science 315:612–617

Boyd PW, Arrigo KR, Strzepek R, van Dijken GL (2012) Mapping phytoplankton iron utilization: insights into Southern Ocean supply mechanisms. J Geophys Res 117:C06009

Briggs N, Perry MJ, Cetinić I, Lee C, D'Asaro E, Gray AM, Rehm E (2011) High-resolution observations of aggregate flux during a sub-polar North Atlantic spring bloom. Deep-Sea Res 58:1031–1039

Cassar N, Bender ML, Barnett BA, Fan S, Moxim WJ, Levy H II, Tilbrook B (2007) The Southern Ocean biological response to Aeolian iron deposition. Science 317: 1067–1070

Ebersbach F, Assmy P, Martin P, Schulz I, Wolzenburg S, Nöthig EM (2014) Particle flux characterisation and sedimentation patterns of protistan plankton during the iron fertilization experiment LOHAFEX in the Southern Ocean. Deep Sea Res I 89:94–103

Eccleston-Parry JD, Leadbeater BSC (1994) A comparison of the growth kinetics of six marine heterotrophic nanoflagellates fed with one bacterial species. Mar Ecol Prog Ser 105:167–177

Egge JK, Aksnes DL (1992) Silicate as regulating nutrient in phytoplankton competition. Mar Ecol Prog Ser 83: 281–289

Fenchel T (1987) Ecology of Protozoa: the biology of free-living phagotrophic protists. Science Tech Publishers, Madison, WI

Finenko ZZ, Hoepffner N, Williams R, Piontkovski SA (2003) Phytoplankton carbon to chlorophyll *a* ratio: response to light, temperature and nutrient. Mar Ecol J II:40–64

Flynn KJ, Stoecker DK, Mitra A, Raven JA and others (2013) Misuse of the phytoplankton-zooplankton dichotomy: the need to assign organisms as mixotrophs within plankton functional types. J Plankton Res 35:3–11

Frada MJ, Bidle KD, Probert I, de Vargas C (2012) In situ survey of life cycle phases of the coccolithophore *Emiliania huxleyi* (Haptophyta). Environ Microbiol 14: 1558–1569

Gervais F, Riebesell U, Gorbunov MY (2002) Changes in primary productivity and chlorophyll *a* in response to iron fertilization in the Southern Polar Frontal Zone. Limnol Oceanogr 47:1324–1335

Giovannoni SJ, Vergin KL (2012) Seasonality in ocean microbial communities. Science 335:671–676

Hamm C, Smetacek V (2007) Armor: why, when, and how. In: Falkowski PG, Knoll AH (eds) Evolution of primary producers in the sea. Elsevier Academic Press, Burlington, p 311–332

Hamm CE, Simson DA, Merkel R, Smetacek V (1999) Colonies of *Phaeocystis globosa* are protected by a thin but tough skin. Mar Ecol Prog Ser 187:101–111

Henjes J, Assmy P, Klaas C, Verity P, Smetacek V (2007a) Response of microzooplankton (protists and small copepods) to an iron-induced phytoplankton bloom in the Southern Ocean (EisenEx). Deep Sea Res I 54:363–384

Henjes J, Assmy P, Klaas C, Smetacek V (2007b) Response of the larger protozooplankton to an iron-induced phytoplankton bloom in the Polar Frontal Zone of the Southern Ocean (EisenEx). Deep Sea Res I 54:774–791

Hillebrand H, Dürselen CD, Kirschtel D, Pollingher U, Zohary T (1999) Biovolume calculation for pelagic and

benthic microalgae. J Phycol 35:403–424
Hoppe CJM, Klaas C, Ossebaar S, Soppa MA and others (2017) Controls of primary production in two phytoplankton blooms in the Antarctic Circumpolar Current. Deep Sea Res II 138:63–73
Irigoien X, Flynn KJ, Harris RP (2005) Phytoplankton blooms: a 'loophole' in microzooplankton grazing impact? J Plankton Res 27:313–321
Iversen MH, Pakhomov EA, Hunt BPV, van der Jagt H, Wolf-Gladrow D, Klaas C (2017) Sinkers or floaters? Contribution from salp pellets to the export flux during a large bloom event in the Southern Ocean. Deep Sea Res II 138:116–125
Jacobson DM (1999) A brief history of dinoflagellate feeding research. J Eukaryot Microbiol 46:376–381
Klaas C (1997) Microprotozooplankton distribution and their potential grazing impact in the Antarctic Circumpolar Current. Deep Sea Res II 44:375–393
Knap AH, Michaels A, Close AR, Ducklow H, Dickson AG (1996) Protocols for the joint global ocean flux study (JGOFS) core measurements. JGOFS Rep 19. Reprint of the IOC Manuals and Guides No. 29, UNESCO, Paris
Laglera LM, Tovar-Sánchez A, Iversen MH, Gonzalez HE and others (2017) Iron partitioning during LOHAFEX: copepod grazing as a major driver for iron recycling in the Southern Ocean. Mar Chem 196:148–161
Lampitt RS (1985) Evidence for the seasonal deposition of detritus to the deep-sea floor and its subsequent resuspension. Deep Sea Res I 32:885–897
Landry MR, Constantinou J, Latasa M, Brown SL, Bidigare RR, Ondrusek ME (2000a) Biological response to iron fertilization in the eastern equatorial Pacific (IronEx II). III. Dynamics of phytoplankton growth and microzooplankton grazing. Mar Ecol Prog Ser 201:57–72
Landry MR, Ondrusek ME, Tanner SJ, Brown SL and others (2000b) Biological response to iron fertilization in the eastern equatorial Pacific (IronEx II). I. Microplankton community abundances and biomass. Mar Ecol Prog Ser 201:27–42
Le Quéré C, Buitenhuis ET, Moriarty R, Alvain S and others (2016) Role of zooplankton dynamics for Southern Ocean phytoplankton biomass and global biogeochemical cycles. Biogeosciences 13:4111–4133
Legendre P, Legendre LF (2012) Numerical ecology, Vol 24, 3rd edn. Elsevier, Amsterdam
Martin JH (1990) Glacial interglacial CO_2 change: the iron hypothesis. Paleoceanography 5:1–13
Martin P, Rutgers van der Loeff M, Cassar N, Vandromme P and others (2013) Iron fertilization enhanced net community production but not downward particle flux during the Southern Ocean iron fertilization experiment LOHAFEX. Global Biogeochem Cycles 27:871–881
Mazzochi MG, González HE, Vandromme P, Borrione I and others (2009) A non-diatom plankton bloom controlled by copepod grazing and amphipod predation: preliminary results from the LOHAFEX iron-fertilization experiment. GLOBEC Int Newsl October 2009:1–4
Menden-Deuer S, Lessard EJ (2000) Carbon to volume relationships for dinoflagellates, diatoms and other protist plankton. Limnol Oceanogr 45:569–579
Moore CM, Mills MM, Arrigo KR, Berman-Frank I and others (2013) Processes and patterns of oceanic nutrient limitation. Nat Geosci 6:701–710
Prowe AEF, Pahlow M, Dutkiewicz S, Follows M, Oschlies A (2012) Top-down control of marine phytoplankton diversity in a global ecosystem model. Prog Oceanogr 101: 1–13
Raiswell R, Benning LG, Davidson L, Tranter M (2008) Nanoparticulate bioavailable iron minerals in icebergs and glaciers. Mineral Mag 72:345–348
Resing JA, Sedwick PN, German CR, Jenkins WJ, Moffett JW, Sohst BM, Tagliabue A (2015) Basin-scale transport of hydrothermal dissolved metals across the South Pacific Ocean. Nature 523:200–203
Richardson TL, Jackson GA (2007) Small phytoplankton and carbon export from the surface ocean. Science 315: 838–840
Sarmiento JL, Gruber N, Brzezinski MA, Dunne JP (2004) High-latitude controls of thermocline nutrients and low latitude biological productivity. Nature 427:56–60
Sathyendranath S, Stuart V, Nair A, Oka K and others (2009) Carbon-to-chlorophyll ratio and growth rate of phytoplankton in the sea. Mar Ecol Prog Ser 383:73–84
Sathyendranath S, Grant M, Brewin RJW, Brockmann C and others (2018) ESA Ocean Color Climate Initiative (Ocean_Colour_cci): Version 3.1 data. Centre for Environmental Data Analysis
Scharek R, Latasa M, Karl DM, Bidigare RR (1999) Temporal variations in diatom abundance and downward vertical flux in the oligotrophic North Pacific Gyre. Deep Sea Res I 46:1051–1075
Sherr EB, Sherr BF (2002) Significance of predation by protists in aquatic microbial food webs. Antonie Leeuwenhoek 81:293–308
Sherr EB, Sherr BF (2009) Capacity of herbivorous protists to control initiation and development of mass phytoplankton blooms. Aquat Microb Ecol 57:253–262
Sieburth JM, Smetacek V, Lenz J (1978) Pelagic ecosystem structure: heterotrophic compartments of the plankton and their relationship to plankton size fractions. Limnol Oceanogr 23:1256–1263
Smetacek V (1981) The annual cycle of protozooplankton in the Kiel Bight. Mar Biol 63:1–11
Smetacek V (1984) Growth dynamics of a common Baltic protozooplankter: the ciliate genus *Lohmanniella.* Limnologica 15:371–376
Smetacek V (1998) Diatoms and the silicate factor. Nature 391:224–225
Smetacek V (2012) Making sense of ocean biota: how evolution and biodiversity of land organisms differ from that of the plankton. J Biosci 37:589–607
Smetacek V, Naqvi SWA (2010) The expedition of the research vessel 'Polarstern' to the Antarctic in 2009 (ANT-XXV/3-LOHAFEX). Rep Pol Mar Res 613/2010. https://epic.awi.de/29569/
Smetacek V, von Bodungen B, Knoppers R, Peinert R, Pollehne F, Stegmann P, Zeitzschel B (1984) Seasonal stages characterizing the annual cycle of an inshore pelagic system. Rapp PV Reùn Cons Int Explor Mer 183:126–135
Smetacek V, Assmy P, Henjes J (2004) The role of grazing in structuring Southern Ocean pelagic ecosystems and biogeochemical cycles. Antarct Sci 16:541–558
Smetacek V, Klaas C, Strass VH, Assmy P and others (2012) Deep carbon export from a Southern Ocean iron-fertilized diatom bloom. Nature 487:313–319
Stoecker DK, Hansen PJ, Caron DA, Mitra A (2017) Mixotrophy in the marine plankton. Annu Rev Mar Sci 9:311–335
Strom SL (2008) Microbial ecology of ocean biogeochemistry: a community perspective. Science 320:1043–1045
Thiele S, Fuchs BM, Ramaiah N, Amann R (2012) Microbial community response during the iron fertilization experiment LOHAFEX. Appl Environ Microbiol 78:8803–8812
Thiele S, Wolf C, Schulz IK, Assmy P, Metfies K, Fuchs BM (2014) Stable composition of the nano- and picoplankton

community during the ocean iron fertilization experiment LOHAFEX. PLOS ONE 9:e113244

Throndsen J (1995) Estimating cell numbers. In: Hallegraeff GM, Anderson DM, Cembella AD (eds) Manual on harmful marine microalgae. UNESCO, Paris, p 63–80

Trainer VL, Bates SS, Lundholm N, Thessen AE, Cochlan WP, Adams NG, Trick CG (2012) *Pseudo-nitzschia* physiological ecology, phylogeny, toxicity, monitoring and impacts on ecosystem health. Harmful Algae 14:271–300

Tréguer P, Bowler C, Moriceau B, Dutkiewicz S and others (2018) Influence of diatom diversity on the ocean biological carbon pump. Nat Geosci 11:27–37

Utermöhl H (1958) Zur Vervollkommnung der quantitativen Phytoplankton-Methodik. Mitt Int Ver Limnol 9:1–38

Venables HJ, Meredith MP (2009) Theory and observations of Ekman flux in the chlorophyll distribution downstream of South Georgia. Geophys Res Lett 36:L23610

Wadley MR, Jickells TD, Heywood KJ (2014) The role of iron sources and transport for Southern Ocean productivity. Deep Sea Res I 87:82–94

Ward BA, Follows MJ (2016) Marine mixotrophy increases trophic transfer efficiency, mean organism size, and vertical carbon flux. Proc Natl Acad Sci USA 113:2958–2963

Wassmann P (1997) Retention versus export food chains: processes controlling sinking loss from marine pelagic systems. Hydrobiologia 363:29–57

Weisse T, Scheffel-Möser U (1990) Growth and grazing loss rates in single-celled *Phaeocystis* sp. (Prymnesiophyceae). Mar Biol 106:153–158

Wu SY, Hou S (2017) Impact of icebergs on net primary productivity in the Southern Ocean. Cryosphere 11:707–722

Xu N, Tang YZ, Qin J, Duan S, Gobler CJ (2015) Ability of the marine diatoms *Pseudo-nitzschia multiseries* and *P. pungens* to inhibit the growth of co-occurring phytoplankton via allelopathy. Aquat Microb Ecol 74:29–41

Zar JH (1999) Biostatistical analyses. Prentice-Hall, Upper Saddle River, NJ

Zingone A, Forlani G, Percopo I, Montresor M (2011) Morphological characterization of *Phaeocystis antarctica* (Prymnesiophyceae). Phycologia 50:650–660

Editorial responsibility: Antonio Bode, A Coruña, Spain

Submitted: November 15, 2017; Accepted: June 28, 2018
Proofs received from author(s): July 26, 2018